Journal of Industrial and Engineering Chemistry xxx (xxxx) xxx

Contents lists available at ScienceDirect

Journal of Industrial and Engineering Chemistry

journal homepage: www.elsevier.com/locate/jiec

Interference of oxygen during the solution combustion synthesis process of ZnO particles: Experimental and data modeling approaches

E. Garmroudi Nezhad [a,1], F. Kermani [a,1], Z. Mollaei [a], M. Mashreghi [b], J. Vahdati Khakhi [a], S. Mollazadeh [a,*]

[a] Department of Materials Engineering, Faculty of Engineering, Ferdowsi University of Mashhad (FUM), Azadi Sq, Mashhad, Iran
[b] Department of Biology, School of Science, Ferdowsi University of Mashhad, 91775-1436 Mashhad, Iran

ARTICLE INFO

Article history:
Received 28 July 2021
Revised 27 September 2021
Accepted 26 November 2021
Available online xxxx

Keywords:
Oxygen interference
Calculation model
Density functional theory
Solution combustion synthesis
Zinc oxide

ABSTRACT

In the present study, the ratio of reducing to oxidizing (F/O) elements as an indicator for maximum oxygen interference during the solution combustion synthesis (SCS) process of ZnO particles was determined using simple mathematical calculations. The obtained result was called special point (S.P). To interpret the role of S.P in the SCS reactions, ZnO particles were synthesized in the presence of citric acid, hexamine, hydrazine, and urea with various F/O values (0.75, 1, 1.25). The correlations between the S.P, physicochemical properties of the synthesized ZnO powders, and density functional theory (DFT) predictions were investigated. X-ray diffraction results, band-gap values, oxygen vacancy data, DFT results, and S.P points demonstrated the direct relation of these parameters. According to the S.P idea, it can be affirmed that the structural defects, particle size, optical band-gap (E_g = 3.06), the color of the products, the magnetic properties (0.2 emu/g), and the antibacterial inhibitory (15.625 μg/mL) of the synthesized particles were controlled via the interference of O_2 during the synthesis process. In fact, the S.P investigation was suggested that the reaction rate of the combustion synthesis process could regulate the properties of ZnO particles.

Introduction

Solution combustion synthesis (SCS) technique is a fast and well-known process that is used widely for the synthesis of oxides through an exothermic reaction between fuel(s) (e.g., glycine, urea) and oxidizer (s) (e.g., $Zn(NO_3)$, $Fe(NO_3)$) in an aqueous media [1–3]. The fuel type and the ratio of reducing to oxidizing elements (F/O) directly affected on the thermodynamics properties of the SCS procedure, i.e., enthalpy, the highest reachable temperature (Tad), and the time (rate) of the combustion reaction [4–7]. The term F/O shows the total ratio of reducing to oxidizing elements. Molar fractions of raw materials are calculated based on Eq. (1) and favorable F/O as follows [8]:

$$F/O = \frac{\sum(\textit{coefficient of reducing elements}) \times \textit{reducing valency} \times \textit{molar fraction}}{(-1)\sum(\textit{coefficient of oxidizing elements}) \times \textit{oxidizing valency molar fraction}} \quad (1)$$

where reducing elements are hydrogen, carbon, and metallic cations with the corresponding valance (v) of +1, +4, and v (e.g., v is +2 for Zn^{2+}), respectively. Besides, oxygen as an oxidizing agent has a valency of −2 [8]. Accordingly, based on the different F/O values, Reaction I is obtained as follows:

$$(x)A(NO_3)_{d1}(s) + (y)\text{Fuel}\ (s) = A_xO_{xd1}\ (s) + fH_2O(g) + gCO_2\ (g) + hN_2(g) \pm iO_2(g) + \textit{heatReactionI}$$

where d1 is the cationic capacity of oxidizer and x, y, f, g, h, and i are the molar coefficients of the reactants. Besides, iO_2 is the amount of interfered O_2 in the SCS reaction. The mentioned coefficient, i.e., x, y, f, g, h, and i in Reaction I, were commonly represented as a function of F/O value with a polynomial order of one or two. To avoid misunderstanding, it should be mentioned that based on Eq. (1) and Reaction I, the term F in the F/O equation (Eq. (1)) is not just referred to the molar fraction of fuel, i.e., y (Reaction I). In fact, it is referred to the reducing elements.

In the SCS method, when F/O = 1, it means that theoretically the combustion reaction does not need atmospheric oxygen and the oxygen molecules of the reactants, i.e., oxygen molecules of the NO_3 groups and other oxidant agents, would be sufficient for the combustion process, i.e., combustion of fuels and oxidation of nitrate(s) [8]. While, when F/O < 1 and F/O > 1, it means that the

* Corresponding author.
E-mail address: Mollazadeh.b@um.ac.ir (S. Mollazadeh).
[1] These authors contributed equally.

https://doi.org/10.1016/j.jiec.2021.11.047
1226-086X/

concentration of oxygen molecules is higher and lower than the amount which is needed for the efficient combustion reaction, respectively [8]. However, oxygen could be interfered in the SCS reaction at all F/O values (F/O = 1, F/O < 1, and F/O > 1) [4,10]. To synthesize Fe_3O_4, Aali et al. [5,10] used different fuels type and F/O values (F/O = 1, F/O < 1, and F/O > 1). The obtained results showed that the Fe_3O_4 phase was not crystallized in any of the designed systems, while, due to the interference of O_2, FeO and Fe_2O_3 were crystallized. To overcome this problem, a vacuum system was proposed to solve the oxidative condition, and finally Fe_3O_4 was successfully synthesized. The main factor for the successful synthesis of Fe_3O_4 was controlling the interference of O_2 during the combustion reaction, which could not be controlled completely only by changing the F/O values. As previously published results have shown interference of O_2 could change thermodynamics and the rate of the combustion reaction. As a result, the properties of the synthesized particles could be changed. Understanding the changes in the function of i (Reaction I) or the amount of interfered O_2 could help predict the properties of SCS reactions, such as adiabatic temperature. Besides, different fuels with various physicochemical properties directly affect the SCS reaction parameters and interference of O_2 [2,10]; investigation of the possible changes in the function of y, which directly refer to the molar fraction of fuel (Reaction I) could help in this regard. It can be hypothesized that calculating the molar ratio of i to y (Reaction I) or oxygen molar coefficient to fuel molar coefficient, that are both could be represented as a function of F/O, provides some new and helpful information about SCS reactions.

The published results of the previous studies imply the interesting photocatalytic performance, antibacterial, and biological activities of the SCS products; the defects, especially oxygen vacancies formed during the SCS reaction, improve products' properties compared to counterparts which were synthesized by other approaches such as sol–gel [11,12]. The oxygen vacancies formed on the surface of the synthesized oxide via the SCS approach due to unusual conditions of the synthesis process, such as high vacuum ($\sim 10^{-20}$ Pa). Previously, the effects of these parameters on the concentration of oxygen vacancies were reported through a simple thermodynamic model [9]. Verification of the previous model using computational studies could provide valuable knowledge about the SCS reactions for future studies. In this view, density functional theory (DFT) has been suggested as a powerful structural modeling approach in particular atoms [13–15]. The relation between the amount of interference of O_2, the previously proposed thermodynamic model, and the DFT calculations could be used to shed light on the effect of variation of the interference of O_2 in the SCS reaction.

ZnO is a bio-safe material with promising antibacterial activity, optical properties, and photocatalytic performance [16–18]. Various methods could be used to synthesis ZnO particles, such as sol–gel, solution combustion, hydrothermal, wet chemical, and physical vapor deposition [4,19]. Among these methods, the solution combustion synthesis (SCS) route is an efficient, straightforward, and fast method due to its low synthesis temperature, precise control of the chemistry, and low cost [8]. Controlling the parameter of the SCS method, i.e., type of fuel and the ratio of fuel to oxidizer/s (F/O), directly impacts the self-sustained exothermic process of SCS reaction. Besides, ZnO is a univalent oxide, and controls of the SCS process parameters of its synthesis are simple, as reported elsewhere [20–23].

The current study tried to investigate the effect of the variation of the molar fraction of interfered O_2 to the molar fraction of fuels as the function of the F/O ratio in the SCS reaction. The presented theoretical studies provide a depth knowledge about the SCS reaction and its relation with the experimental procedure. Besides, this study attempts to investigate the correlation between the theoretical studies and the physicochemical properties and *in vitro* antibacterial performance of the SCS synthesized ZnO particles. The phase and the optical properties of SCS synthesized ZnO powders were predicted using DFT, and their correlations with the interference of O_2 and the defects were clarified in the current study.

Experimental procedure

Synthesis of ZnO particles

Zinc nitrate ($Zn(NO_3)_2.6H_2O$ 98.0%, M.W 297.49, Merck, Germany), citric acid ($C_6H_8O_7$ 99.5%, M.W 192.124, Merk, Germany), hydrazine (N_2H_4 64–65%, M.W 32.04, Merk, Germany), hexamine ($C_6H_{12}N_4$ 99%, M.W 140.19. Merk, Germany), and urea ($CO(NH_2)_2$, 97%, M.W 94.07, Merck, Germany), were used as the raw materials. As mentioned before, F/O values are determined using Eq. (1) (Eq. (1)) [8]:

$$\text{Eq. (1): } F/O = \frac{\sum (\text{coefficient of reducing elements}) \times \text{reducing valency} \times \text{molar fraction}}{(-1)\sum (\text{coefficient of oxidizing elements}) \times \text{oxidizing valency} \times \text{molar fraction}}$$

The reducing and oxidizing valence of the reactants which were used in the current study could be calculated based on the information represented in Table 1.

The exact amounts of raw materials were calculated based on the following steps:

Step 1: The coefficient of one (1) is considered for the oxidizing agent (here $Zn(NO_3)_2$), and the coefficient (n) is considered for the reducing agents (here citric acid, hydrazine, hexamine, and urea). For example, to synthesis ZnO powders in the presence of citric acid, F/O is calculated as follows:

$$\frac{F}{O} = \frac{(1(\nu Zn) + 6 * 2(\nu H) + (6n(\nu C) + 8n\ (\nu H)}{(-1)(6(\nu O_2) + 6 * (\nu O_2) + (7n(\nu O_2)} = \frac{14 + 32\ n}{24 + 14\ n}$$

Step 2: n is calculated based on the favorable F/O value. This F/O could be selected based on the literature reviews.

Step 3: The SCS reaction should be balanced based on the calculated value of n in step 2. It needs to be noted that to balance SCS reaction at F/O > 1, O_2 should be added in the reactant side, whereas when F/O < 1, O_2 should be added in the products side. In this study, the reactions were balanced using the GEM module of the HSC chemistry software package [24].

Table 2 shows the calculations mentioned above for the synthesis of ZnO powders in the presence of citric acid, hydrazine, hexamine, and urea as fuels.

After the reaction was balanced, the coefficient equations are calculated based on the used F/O ratio (X), which is equal to 0.75, 1, and 1.25 in all systems and the obtained results are presented as follows:

Table 1
The reducing and oxidizing valence of the utilized reactants in this study.

Reactants	Role	Reducing valance calculation	Reducing valance
citric acid ($C_6H_8O_7$)	Reducing agent	6 (+4) + 8 (+1) + 7 (−2) = 18	18
hexamine ($C_6H_{12}N_4$)	Reducing agent	6 (+4) + 12 (+1) + 4 (0) = 36	36
hydrazine (N_2H_4)	Reducing agent	2 (0) + 4 (1) = 4	4
urea ($CO(NH_2)_2$)	Reducing agent	1 (+4) + 1(−2) + 2 (0) + 4 (1) = 6	6
$Zn(NO_3)_2$	Oxidizing agent	1 (+2) + 2 (0) + 6 (−2) = −10	−10

System I: (Fuel: citric acid)

Reaction II: $Zn(NO_3)_2.6H_2O + (1.419X^2 - 1.004X + 0.1404)\ C_6H_8O_7 = ZnO + (5.643X^2 - 4.046X + 6.577)H_2O + N_2 + (8.547X^2 - 6.086X + 0.8724)CO_2 + (-2.416X^2 - 4.424X + 6.84)O_2$

System II: (Fuel: hexamine)

Reaction III: $Zn(NO_3)_2.6H_2O + (-0.004X^2 + 0.6746X - 0.3926)C_6H_{12}N_4 = ZnO + (4X + 3.667)H_2O + (-0.008X^2 + 1.344X + 0.2148)N_2 + (-0.0016X^2 + 4.003X - 2.335)CO_2 + (0.004X^2 - 6.007X + 6.003)O_2$

System III: (Fuel: hydrazine)

Reaction IV: $Zn(NO_3)_2.6H_2O + (6XX - 3.5)\ N_2H_4$ = ZnO + $(12X - 1)H_2O + (6X - 2.5)N_2 + (6X - 6)O_2$

System IV: (Fuel: urea)

Reaction V: $Zn(NO_3)_2.6H_2O + (1.524X^2 + 1.539X - 1.396)CH_4N_2O = ZnO + (-4.136X^2 + 19.25X - 5.778)H_2O + (1.524X^2 - 1.539X - 0.396)N_2 + (1.524X^2 + 1.534X - 1.396)CO_2 + (5.346X^2 - 17.46X + 12.12)O_2$

In this study, the equations were calculated using MATLAB software (R 2018b). In the curves fitting settings, the R-squared (R^2) of the equations was set to 1, and then the curves were fitted. It needs to be noted that commonly the equation with polynomial order of one or two with the maximum R^2 is recommended.

According to the chemical reactions in system I–IV, to obtain 0.01 mol of ZnO powder, 0.01 mol zinc nitrate was completely dissolved in 5 mL of deionized water (Cas number: 7732-18-5) using a 25 mL beaker under constant stirring (1000 rpm) in room temperature. The appropriate amount of each fuel was dissolved in 5 mL of deionized water in the 25 mL beaker, separately. According to each reaction, the fuel-containing solution was added to the nitrate solution with a dro1p rate of 30 drops/min. Then, the obtained solution was homogenized with continuous stirring with 1000 rpm for 10 min. Prepared solutions were transferred into 100 mL alumina crucible and then heated up to about 330 °C using a digital hot-plate (Alfa, D500, Iran, plate diameter of 20 cm). Over time, water was evaporated and the solution became viscous. Finally, the combustion reaction was ignited spontaneously, resulting in the formation of solid powders. It should be mentioned that the yield of the SCS process in the current study was lower than 40% for all systems.

Combustion temperatures (T_c) and reaction time (R_t) of all reactions were defined by USB-4718 (Advantech Co., Ltd) data acquisition. Besides, combustion enthalpy and adiabatic temperature (T_{ad}) were determined using the HSC chemistry® software package [24].

The special point (S.P) was calculated as follows:

Step 1: Plotting the homographic graph of Y versus X, in which Y is equal to $-\frac{O.C}{F.C}$ $(Y = -\frac{O.C}{F.C})$

where O.C and F.C are oxygen and fuel molar coefficients in systems I–IV, respectively.

It should be mentioned that O.C and F.C are both calculated and presented as the function of F/O.

Step 2: Determining the vertical asymptote(s) of the plotted curves. Calculation of the vertical asymptote(s) can be considered in two different cases:

*) The denominator of the fraction, i.e., the fuel molar coefficient, is zero. Although this assumption is mathematically correct, the SCS process is not possible in this case.

**) The numerator of the fraction, i.e., the oxygen molar coefficient, approaches infinity. It means the interference of oxygen could have a maximum value at this F/O value. In this study, assumption ** was acceptable from mathematical and thermodynamical points of view.

Accordingly, the obtained value from vertical asymptote(s) was used to calculate the S.P; S.P value could be equal to the average of the vertical asymptote values with the bellow rules. These rules were used to define the mathematical homographic function by considering the thermodynamic of SCS reactions.

(a) In the curves with two positive vertical asymptotes, the average values of the vertical asymptote could be considered as the S.P.
(b) In the curves with a negative vertical asymptote and a positive vertical asymptote, if the average of these vertical asymptotes is a positive number, the average would be equal to the S.P, while when the average of vertical asymptote is a negative number, the S.P could not be defined.
(c) In the curves with a positive vertical asymptote, the S.P value would be equal to the vertical asymptote value.
(d) In the curves with a negative vertical asymptote, the S.P value could not be defined.

In the current study, each chosen fuel corresponded to one of the rules mentioned above. It should be mention that when the average of the vertical asymptote is a negative number, it means the fuel(s) would be available as an impurity in the products of the SCS reaction.

Table 2
The results of the theoretical calculated fuel to oxidizer (F/O) ratio for conducting the solution combustion synthesis of ZnO powders.

Fuel	Chosen F/O	F/O	n	Balanced reaction
Citric acid	0.75	$\frac{14+32\ n}{24+14\ n}$	0.180	$Zn(NO_3)_2{*}6H_2O + 0.18C_6H_8O_7 = ZnO + 1.08CO_2 + 6.72H_2O + N_2 + 1.69O_2$
	1		0.550	$Zn(NO_3)_2{*}6H_2O + 0.555C_6H_8O_7 = ZnO + 3.333CO_2 + 8.222H_2O + N_2$
	1.25		1.103	$Zn(NO_3)_2{*}6H_2O + 1.103C_6H_8O_7 + 2.465O_2 = ZnO + 6.620CO_2 + 10.412H_2O + N_2$
Hexamine	0.75	$\frac{14+36\ n}{24}$	0.110	$Zn(NO_3)_2{*}6H_2O + 0.111C_6H_{12}N_4 = ZnO + 0.666CO_2 + 6.666H_2O + 1.222\ N_2 + 1.501O_2$
	1		0.277	$Zn(NO_3)_2{*}6H_2O + 0.277C_6H_{12}N_4 = ZnO + 1.662CO_2 + 7.662H_2O + 1.554\ N_2$
	1.25		0.440	$Zn(NO_3)_2{*}6H_2O + 0.444C_6H_{12}N_4 + 1.469O_2 = ZnO + 2.664CO_2 + 8.664H_2O + 1.888\ N_2$
Hydrazine	0.75	$\frac{14+4n}{24}$	1.000	$Zn(NO_3)_2{*}6H_2O + N_2H_4 = ZnO + 8H_2O + 2\ N_2 + 1.5O_2$
	1		2.500	$Zn(NO_3)_2{*}6H_2O + 2.5N_2H_4 = ZnO + 11H_2O + 3.5\ N_2$
	1.25		4.000	$Zn(NO_3)_2{*}6H_2O + 4N_2H_4 + 1.5O_2 = ZnO + 14H_2O + 5\ N_2$
Urea	0.75	$\frac{14+8n}{24+2n}$	0.615	$Zn(NO_3)_2{*}6H_2O + 0.615CH_4N_2O = ZnO + 0.615CO_2 + 7.23H_2O + 1.615\ N_2 + 1.577O_2$
	1		1.666	$Zn(NO_3)_2{*}6H_2O + 1.666CH_4N_2O = ZnO + 1.666CO_2 + 9.332H_2O + 2.666\ N_2$
	1.25		2.909	$Zn(NO_3)_2{*}6H_2O + 2.909CH_4N_2O + 1.863O_2 = ZnO + 2.909CO_2 + 11.818H_2O + 3.909\ N_2$

Characterization

Before the characterization steps, all synthesized samples were ground in an agate mortar for 5 min. The phase compositions of the synthesized powder were investigated by X-ray diffraction (XRD) (Explorer GNR, Italy) by using monochromatic Cu-Kα radiation over the 2θ range of 20–70° with step size 0.02°, and time per step 1 s. Crystallite size of (101) plane of the synthesized powders was estimated using Debey–Scherrer equation (Eq. (2)) [25]:

$$D_{(hkl)} = K\lambda/(\beta_{1/2} * \cos(\theta)) \quad (2)$$

where K is the shape factor, which is equal to 0.9, λ is X-ray wavelength, which is equal to 1.54, $\beta_{1/2}$ is full-width at half-maximum (FWHM), and θ is the Bragg's diffraction angle in degrees.

The micro-strain (ε) of the (101) plane of ZnO was determined by the below equation (Eq. (3)).

$$\varepsilon = \beta_{1/2}\cos(\theta/4) \quad (3)$$

where ε is the amount of micro-strain, and $\beta_{1/2}$ is FWHM.

The particle size, polydispersity index (PDI), and the surface charge of the particles were assessed using a particle size analyzer (HORIBA Scientific, SZ 100, France). To evaluate the particle size, zeta potential and PDI of ZnO particles, 0.01 g of particles were dispersed in absolute ethanol (99.95%) using ultrasonication process (40 kHz, 400 W * 60%). The morphology of the gold sputter-coated particles was characterized using field emission scanning electron microscopy (FESEM) (MIRA3, TESCAN, CZ). Magnetic properties of the synthesized powder were explored using a vibrating sample magnetometer (VSM) analysis at room temperature (Magnetic Danesh Pajoh Inst, Iran). The color coordination of the synthesized powder in a wet state was determined using chroma meters measuring head (CR-400 Head, Japan). The optical properties of the synthesized powders were studied by a UV–Vis spectrophotometer (Hitachi, U-3010, USA) with a scan rate of 100 nm/min. Before the UV–VIS analysis, 0.01 g of CaPs were dispersed in 30 mL deionized water by ultrasonication (40 kHz, 400 W * 40%) for 10 min.

The value of the band-gap energy (E_g) is obtained according to Eq. (VI) [4].

$$\alpha h\nu = B\ (h\nu - \mathrm{Eg})^n \quad (\mathrm{VI})$$

where E_g and n are band-gap energy values and 0.5, respectively. The E_g was achieved from $(\alpha h\nu)^2$ versus $h\nu$ plot.

Computational studies

The effect of the concentration of the oxygen vacancy defects and impurity on the structural and optical properties of the synthesized particles was evaluated using the density functional theory (DFT) via the CASTEP (Cambridge Enterprise Limited, registered number 1069886). For this, ZnO with a hexagonal structure, a space group of $P6_3/mc$, and cell parameters of a = 3.2494 Å and c/a = 1.6014 were built. The calculations were performed based on the generalized gradient approximation (GGA) and PBE_{Sol} with the Hubbard U method as the exchange–correlation potential [26]. The plane-wave cutoff energy and k points mesh was set at 550 eV and 5*5*5, respectively, using the Monkhorst–Pack scheme [27,28]. The geometry convergence of structure with 0.01 eV/Å maximum force (M-F), 0.0005 Å maximum atomic displacement (M-D), and 0.02 GPa maximum stress (M-S) was optimized with the Broyden–Fletcher–Goldfarb–Shanno (BFGS) method [27]. The oxygen vacancy was simulated by reducing an oxygen atom from a 2 × 2 × 1 ZnO supercell and adding a Zn atom. Besides, for simulating the crystalline structure of N-doped ZnO, first, a 2 × 2 × 1 hexagonal wurtzite ZnO supercell was built, and an N atom replaced an O atom. The Hubbard parameters were adjusted as follows: $U_{d,Zn}$ = 10.5, $U_{p,O} = U_{p,N}$ = 7 eV. The effect of oxygen vacancy and doping of nitrogen (N) atom in the structure of the ZnO powders on the XRD peak position were studied using the Mercury 3.8 (The Cambridge Crystallographic Data Centre (CCDC)).

It should be mentioned that the standard computational methods may not be sufficient for ZnO systems, as reported elsewhere [29,30]. Besides, the electronic properties of ZnO can be quite sensitive to basic functions used to calculate ZnO systems. The mentioned parameters are beyond the generalized gradient approach, which was used in this study.

In vitro antibacterial activity

Bacterial cell preparation

The Gram-negative bacterium Escherichia coli (*E. coli*) (PTCC: 1330) and gram-positive bacterium Staphylococcus aureus (*S. aureus*) (PTCC: 1112) were cultured in the nutrient broth (NB) in the incubator with 5% CO_2 at 37 °C for 24 hours. UV–Vis spectrophotometer was employed at 630 nm to measure the optical density (OD) of the overnight cultured bacteria. Subsequently, the overnight culture was diluted using the NB medium to obtain an OD ranged between 0.08 and 0.1 (1.5×10^6 CFU/ mL).

Assessment of cell viability

ZnO particles were dispersed in a solvent. The solvent was composed of deionized water, dimethyl sulfoxide (DMSO), and glycerol with a volume ratio (4:1:1). Then, 100 µL of the obtained suspension with the desired concentrations of 250, 125, 62.5, 31.2, 15.6, 7.8, 3.9, and 1.95 µg/ml along with 100 µL of NB culture medium was transferred in a 96-well microplate. The diluted culture was then seeded into the microplate and incubated at 37 °C for 24 h. The OD at the wavelength of 630 nm was measured using an ELIZA microplate reader (Synergy HT, BioTek, USA). The microplates without the powder and the microplates containing solvents media were considered as a negative control. The antibacterial test was performed three times for each sample, and all of the data were reported as mean ± standard deviation.

Statistical evaluations

The results of particle size, zeta potential, and PDI values were statistically evaluated using a one-way analysis of variance (ANOVA). Probability values less than 0.05 were considered significant ($^*p < 0.05$, $^{**}p < 0.01$, $^{***}p < 0.001$, and $^{****}p < 0.0001$) (GraphPad Prism 8.02 (263), San Diego, California, USA).

Results and discussion

Thermodynamic aspects

Calculation of the special point (S.P)

The S.P points (or the F/O values which resulted in the maximum interference of O_2 in the combustion reaction) in the presence of different fuels were calculated according to the proposed calculation rules (see Section 2.1), and the data are presented in Table 3 and Fig. 1A–D.

According to data, citric acid had two positive vertical asymptotes (0.190, 0.520), and the average of them is 0.355. Accordingly, the S.P for citric acid would be 0.355. When fuel was hexamine, the curve had a positive vertical asymptote (0.580); therefore, the S.P would be equal to the vertical asymptote (0.580). When fuel was hydrazine, the curve had a negative vertical asymptote (−0.580), and the S.P could not be defined according to the proposed rules. Finally, when the fuel was urea, the curve had a negative

Table 3
The results of the calculated special point (S.P) for the utilized fuels.

Fuel	Vertical Asymptote	Average	S. P
Citric acid	0.19, 0.52	0.355	0.355
Hexamine	0.58	–	0.580
Hydrazine	−0.58	–	Not defined
Urea	−1.59, 0.58	−0.505	Not defined

(−1.590) and a positive (0.580) vertical asymptotes with an average of −0.505; thereby, the S.P value could not be defined.

The normalized (comparable) values of S.P (or nS.P, $0 \leq$ nS.P ≤ 1) for the synthesized samples in the presence of citric acid and hexamine for the various F/O ratios were calculated, and the data were presented in Table 4. The calculated data in Table 4 were used throughout the study to investigate S.P's effect on the properties of the synthesized particle. Besides, for the synthesized particle in the presence of hydrazine and urea fuels, which had not a defined S.P value in the current study, the effect of F/O values on the final properties was investigated.

T_c and the R_t and their correlation with S.P

The measured T_c and R_t values are presented in Table 4. The relation between T_c and R_t with nS.P data are presented in Fig. 2A and B, respectively. According to T_c data, during the synthesis process in the presence of citric acid, hexamine, and hydrazine, the highest combustion temperatures were 690 ℃ and 724 ℃, respectively. The T_c in these systems increased with increasing the F/O ratio. The increasing trend of T_c in the mentioned samples could be related to the interference of O_2 during the combustion process. In the synthesized particles in the presence of urea, T_c constantly decreased when the F/O ratio was increased. The urea fuels (S.P = −0.505) and hydrazine (S.P = −0.580) might be remained in SCS products.

The time of reaction in the synthesized samples in the presence of citric acid and hexamine was increased when nS.P increased (Fig. 2B); this relation might be associated with the diluent role of the fuels in the reaction as well as the low amount of interference of O_2 in the combustion reaction at the high S.P values. The reaction time increased in the synthesized samples with hydrazine and urea when F/O increased, as well.

T_{ad} and oxygen vacancy concentrations

To calculate the concentration of oxygen vacancy in the different systems, combustion enthalpy ($\Delta H°_{298}$) and its corresponding T_{ad} of the reactions in system I–IV (see Section 2.1) were calculated and the data were presented in Table 4. As seen in Table 4, the difference between the thermodynamic properties of systems highly depends on the physicochemical properties of fuels and F/O. It should be noted that the formation enthalpy of citric acid, hexamine, hydrazine, and urea are −1390, 125.5, 93.242, −351.375 kJ/-mol, respectively [24]. Besides, as shown in Table 4, the highest T_{ad} in each system is related to the reaction, which is occurred in stoichiometric F/O value, i.e., F/O = 1. As reported elsewhere, the difference between theoretical T_{ad} and the measured T_c is related to the interference of O_2 and energy loss incurred during the combustion process [10].

Based on the Kermani model [9], the relative theoretical concentration of oxygen vacancies was calculated, and the obtained data were presented in Table 4. As shown in Table 4, in the synthesis systems in the presence of different fuels, the concentration of oxygen vacancies increased by decreasing the F/O ratios. The indirect relation of the concentration of the oxygen vacancy defects and S.P is illustrated in Fig. 3; conducted synthesis process with low nS.P values and reaction time (see section 3.1.2) increased the concentration of oxygen vacancy defects. It should be mentioned that according to the previously published results, little difference between the concentration of oxygen vacancies in the various systems could cause a significant difference in physical properties [9,31–34].

The relation of S.P and XRD results

XRD patterns of the synthesized samples are depicted in Fig. 4A. The result of the calculation of the crystallite size and micro-strain values are also shown in Table 5. According to the standard ICDD reference pattern of (36-1451), ZnO with hexagonal structure and space group of $P6_3/mc$ was crystallized almost in all systems. Some minor levels of impurities were detected in the synthesized system in the presence of urea at F/O = 1.25, which could be due to the remained urea in this sample. The combustion reaction process in the presence of urea at F/O = 1.25 was not completed; thereby, the presence of impurities was expected. As shown in

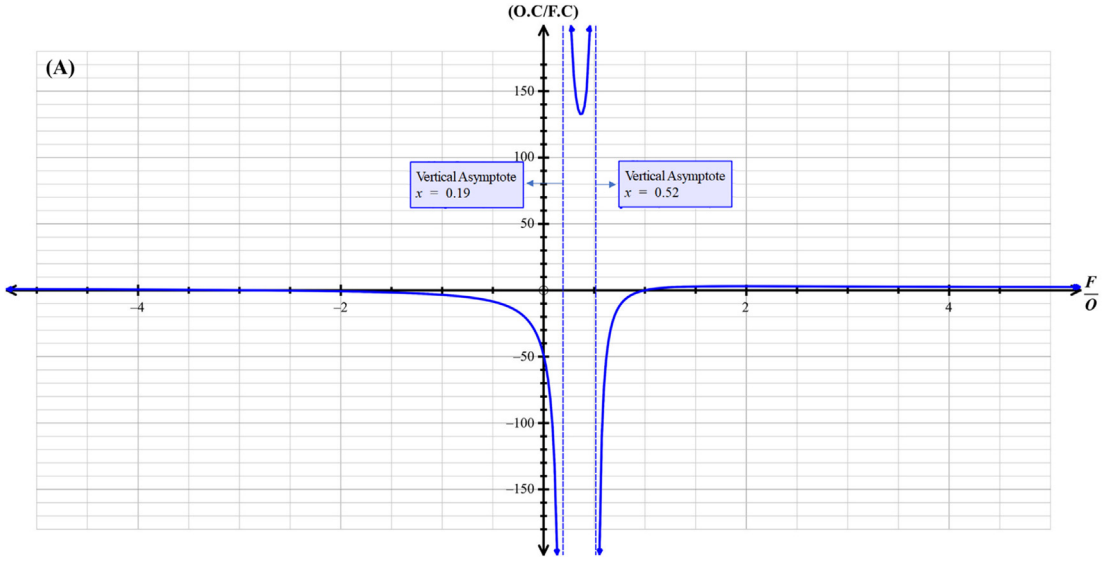

Fig. 1A. The homographic function of oxygen to fuel molar coefficient (O.C/F.C) versus fuel to oxidizer ratio (F/O) in system I for citric acid fuel.

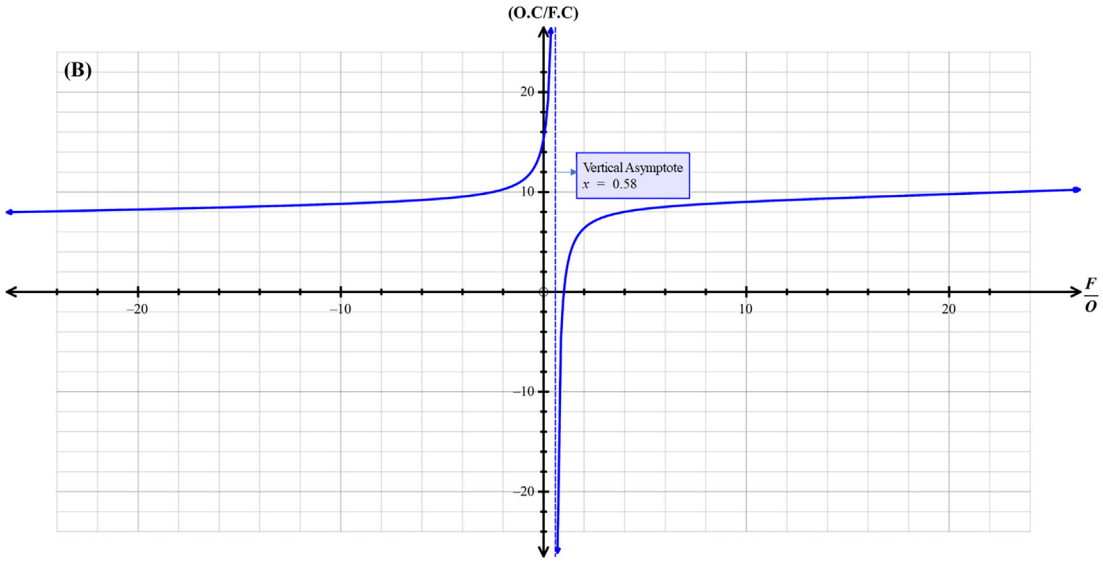

Fig. 1B. The homographic function of oxygen to fuel molar coefficient (O.C/F.C) versus fuel to oxidizer ratio (F/O) in system II for hexamine fuel.

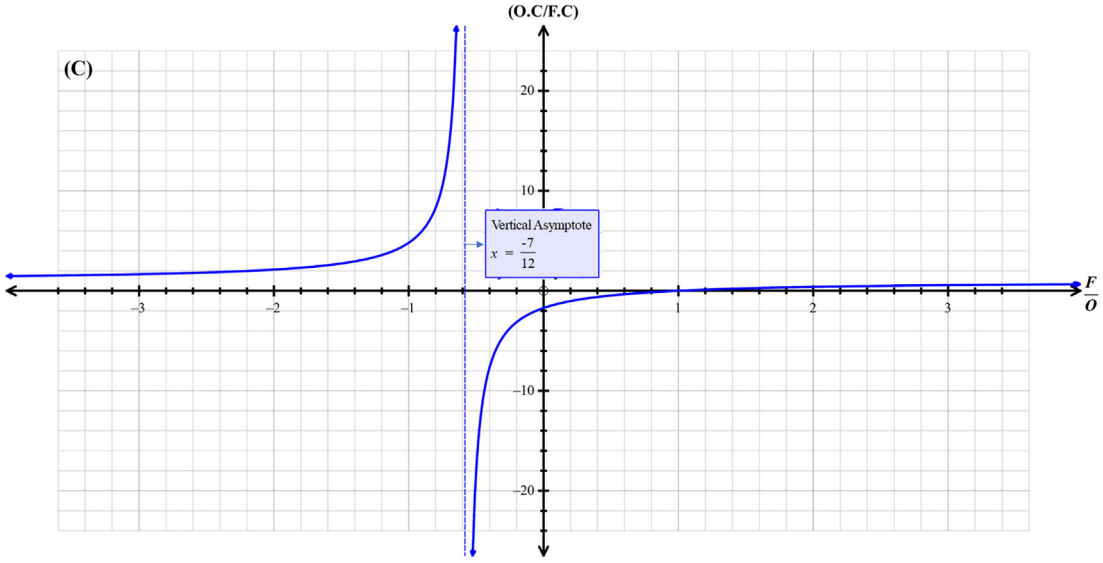

Fig. 1C. The homographic function of oxygen to fuel molar coefficient (O.C/F.C) versus fuel to oxidizer ratio (F/O) in system III for hydrazine fuel.

Table 5, when F/O was increased from 0.75 to 1.25, the crystallite size was increased in all systems. The smallest crystallite size of (100) reflection (38 nm) is related to the synthesized sample using citric acid at F/O = 0.75. Besides, the highest crystallite size (96 nm) is related to the synthesized sample with hydrazine at F/O = 1.25. The crystallite size values increased with increasing the S.P values (Fig. 4B); the formation time of particles with high nS.P is longer due to the low concentration of interfered O_2 in these systems (see Section 3.1) and as a result of which the particle size increased.

The formed lattice during the SCS methods contains super-lattice defects due to the explosive nature of the combustion reaction [35]. The calculated micro-strain values in the synthesized ZnO particles are represented in Table 5. The highest micro-strain is value about 0.084 % in the synthesized powder in the presence of hexamine as fuels at F/O = 0.75. The difference between the crystallite size and micro-strain values of the synthesized samples in the presence of different fuels could be related to the different rates of the combustion process and the combustion temperatures.

Fig. 4C demonstrated the indirect relation of micro-strain and S.P values. According to the represented relation in Fig. 4C, it can be said that when the amount of interference of O_2 in the combustion reaction increased (samples with low S.P values and reaction time), the micro-strain values increased. Besides, as reported elsewhere, the different micro-strain values of the formed lattice in the SCS reaction might be due to the structural defect [9,23,36]. These matters could have a beneficial effect on the ZnO properties (e.g., antibacterial inhibitory).

The correlation between S.P, XRD peak position, and the concentration of oxygen vacancy defects

The XRD peak position relied on the phase properties (e.g., micro-strain) and the structural defects [1]. The surface oxygen vacancy defects significantly affect the XRD peak position in the SCS approaches, as well [1,9]. The XRD peak shift associated with Fig. 4A is illustrated in Fig. S1 (see supplementary information). The different peak shift values for the synthesized samples in the

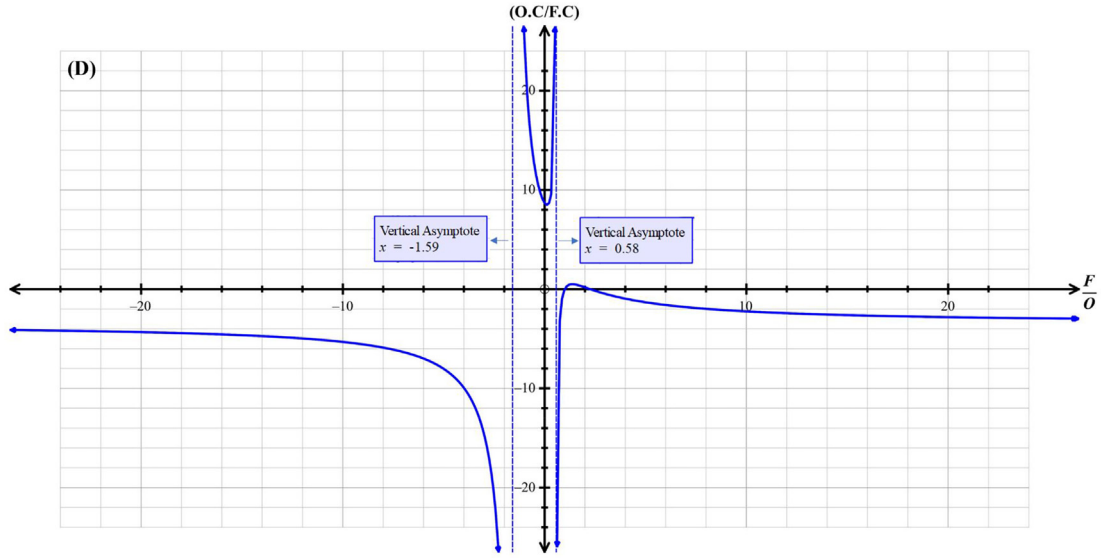

Fig. 1D. The homographic function of oxygen to fuel molar coefficient (O.C/F.C) versus fuel to oxidizer ratio (F/O) in system IV for urea fuel.

Table 4
The results of normalized special point (nS.P), combustion temperature (T_c), reaction time (R_t), enthalpy of reaction ($\Delta H°_{298}$), adiabatic temperature (T_{ad}), and the theoretical concentration of oxygen vacancy defects values. (#These values are relative and could not be compared for different fuels).

Fuel	F/O (X)	Special point (S.P)	(F/O) * (S.P)	Normalized (S.P)	T_c (°C)	R_t (sec)	$\Delta H°_{298}$ (kJ/mol)	T_{ad} (°C)	Oxygen vacancy concentration * 10^{-5} (#)
Citric acid	0.75	0.355	0.266	0.367	554	148	−433.866	1199	2.64
	1		0.355	0.490	641	174	−533.197	1411	2.62
	1.25		0.444	0.612	690	193	−506.021	1353	2.61
Hexamine	0.75	0.580	0.435	0.600	580	186	−261.976	882	2.64
	1		0.580	0.800	625	228	−515.350	1471	2.62
	1.25		0.725	1.00	764	253	−343.710	1072	2.60
Hydrazine	0.75	Not defined	–	–	605	109	−600.274	1476	2.63
	1		–	–	714	136	−819.826	1916	2.62
	1.25		–	–	888	154	−660.561	1597	2.61
Urea	0.75	Not defined	–	–	610	193	−280.293	1007	2.67
	1		–	–	573	224	−378.435	1264	2.65
	1.25		–	–	541	369	−315.044	1098	2.64

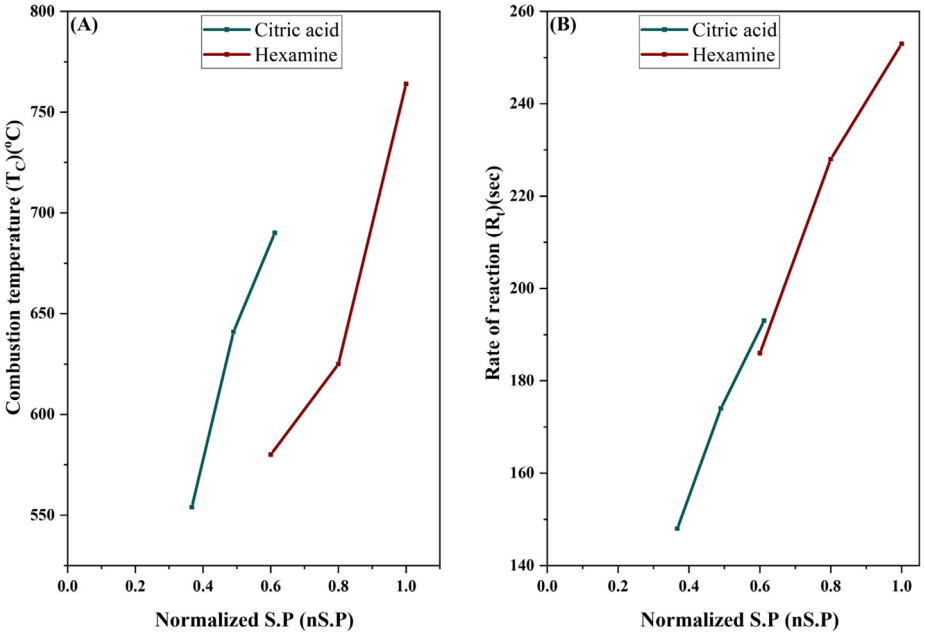

Fig. 2. The correlation between combustion temperature (T_C) (A) and the rate of the SCS reaction (R_t) (B) with the special point (S.P).

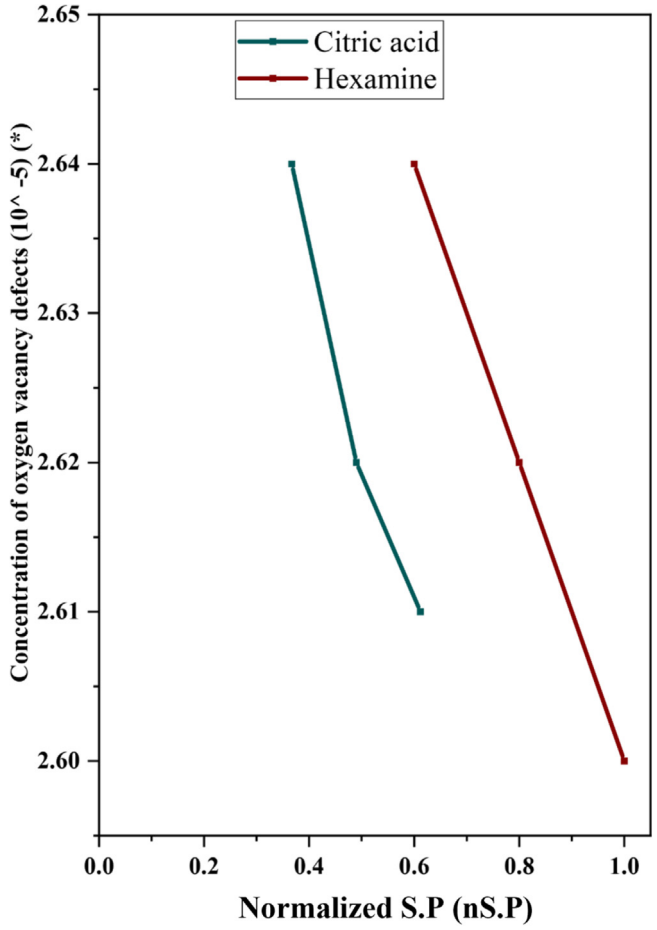

Fig. 3. The correlation between the calculated concentration of oxygen vacancy defects and special point (S.P). # These values are relative and could not be compared for different fuels.

presence of different fuels could be associated with different lattice disordering as a result of high concentration of vacuum in the SCS process and different thermodynamic characteristics of fuels (e.g., combustion enthalpy). The prediction of the XRD peak position as the function of the concentration of the oxygen vacancy defects is shown in Fig. 5A. According to the DFT results in Fig. 5A, the XRD peak positions shifted to higher degrees when the concentration of oxygen vacancies increased. The linear relation between the XRD peak position and DFT was estimated by about $y = 0.322x$, where y is the concentration of oxygen vacancies, and x is the peak shift compared to the standard ICDD reference pattern of ZnO (36-1451). Comparing the obtained results from the Kermani model (Table 4) and the XRD peak position of Fig. S1, which is shown in Fig. 5A, interestingly showed a similar result with DFT methods. According to Fig. 5A, in the synthesized samples in the presence of citric acid, hexamine, and urea as fuels, when the concentration of oxygen vacancies increased, the (101) peak was shifted to higher degrees. While in the synthesized sample in the presence of hydrazine, the (101) peak was shifted to lower degrees; this matter might be related to the doping of nitrogen atom(s) in the ZnO structure, as shown in Fig. S2. Fig. 5B is shown the relation between S.P and XRD peak shift; when the amount of interference of oxygen in the synthesis reaction was increased, the amount of peak shift was enhanced. Comparing Fig. 5A and Fig. 5B demonstrated that the high rate of the synthesis reaction, which resulted from the interference of O_2, could increase the concentration of oxygen vacancy defects and, as a result, change the XRD peaks positions.

Particle size, zeta potential, and PDI

The SCS method, regarding its fast and explosive nature, provides a good opportunity to miniaturize the particle size [37,38]. The results of the particle size, zeta, and PDI of the synthesized powders are presented in Table 6. Significant change in the synthesized samples at F/O = 0.75 and F/O = 1.25 compared to sample synthesized at F/O = 1 was marked in Table 6 $^{*}p < 0.05$, $^{**}p < 0.01$, $^{***}p < 0.001$, and $^{****}p < 0.0001$). As presented in Table 6, overall, the samples synthesized at F/O = 0.75 have a smaller particle size compared to samples synthesized at other F/O values. The lowest particle size (39 nm) is related to the sample synthesized using citric acid at F/O = 0.75. Increasing the F/O values increased the particle size up to 75 nm. The obtained results of the particle size distribution of the synthesized ZnO with the SCS method (without any treatment) are considerable compared to other techniques. The relation between S.P and the particle size in Fig. 6A illustrated that the synthesized samples with the lower S.P, i.e., the synthesized powders with higher interference of O_2 and the

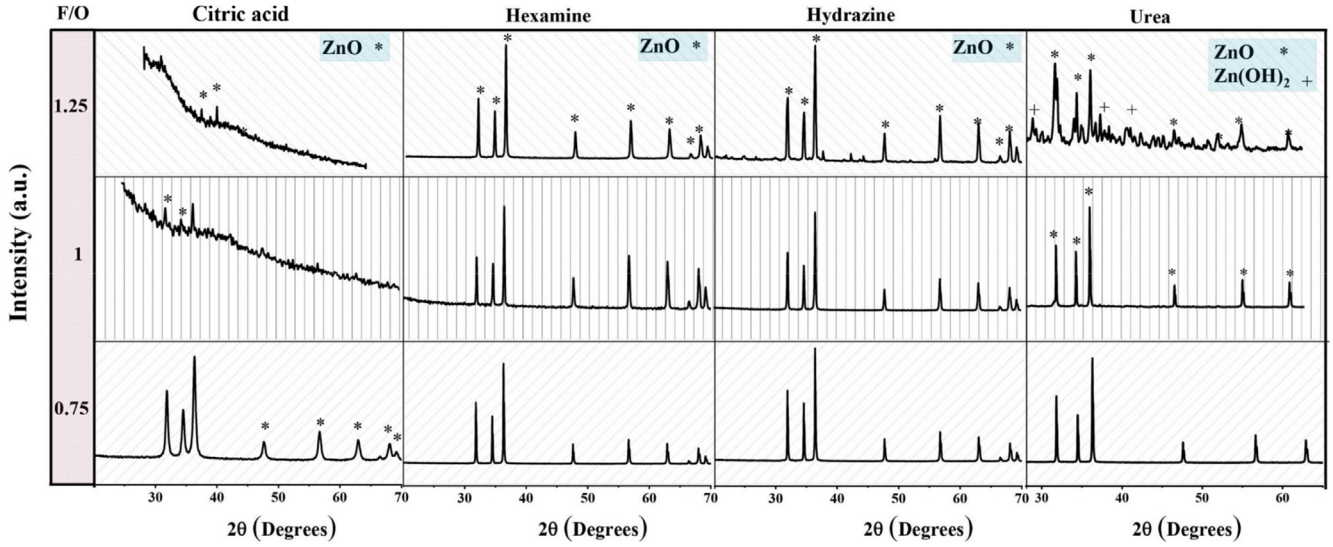

Fig. 4A. X-ray diffraction results of the synthesized ZnO particles.

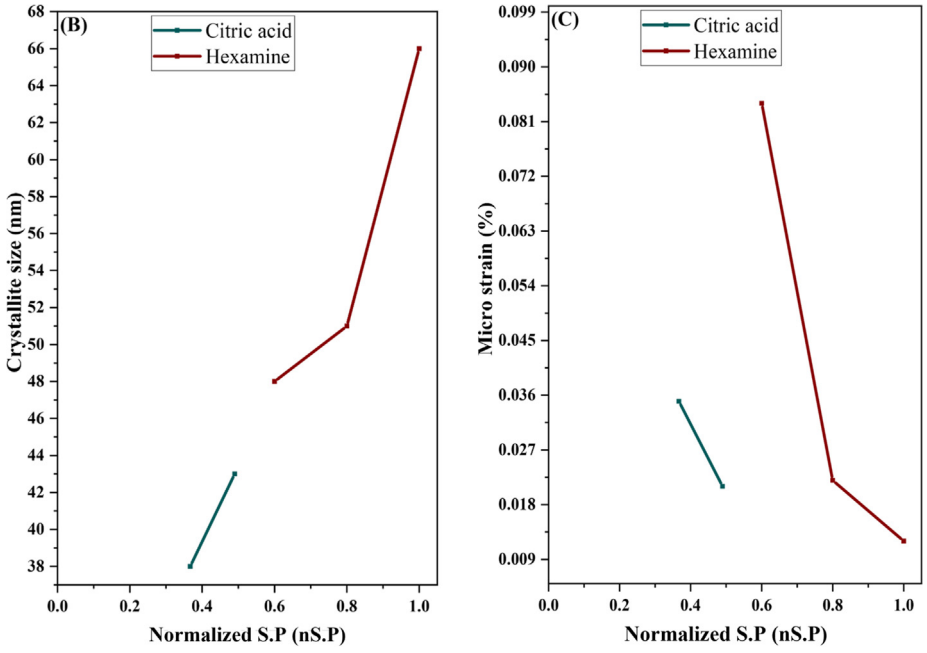

Fig. 4B and C. The correlation between the calculated crystallite size (B) and micro strain (C) with special point (S.P) values.

Table 5
The results of the calculated crystallites size, micro strain, crystallinity, and lattice constant of synthesized ZnO particles in different systems.

Fuel	F/O	Crystallite size of (101) reflection nm	Average crystallite size of (101), (100), and (002) reflections Nm	Micro strain * 10^{-2} %
Citric acid	0.75	38	46	3.5
	1	43	53	2.1
	1.25	Amorphous phase is higher than 75%		
Hexamine	0.75	48	56	8.4
	1	51	59	2.2
	1.25	66	68	1.2
Hydrazine	0.75	50	49	1.6
	1	70	68	0.3
	1.25	96	93	0.1
Urea	0.75	88	89	0.8
	1	91	99	0.4
	1.25	Contains impurities		

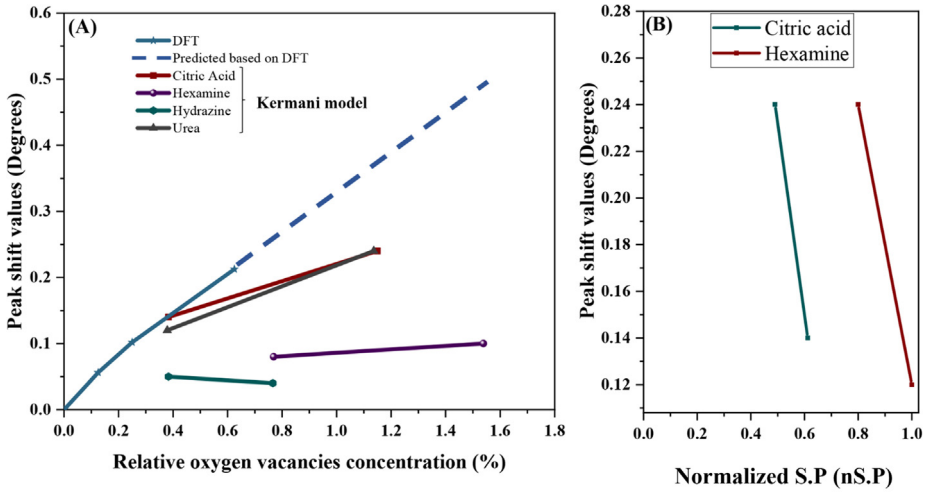

Fig. 5. The correlation between the density functional theory (DFT), X-ray diffraction data of the synthesized ZnO, and the calculated concentration of oxygen vacancy defects with the Kermani model [9] (A). The correlation between the observed peak shift value and special point (S.P) (B).

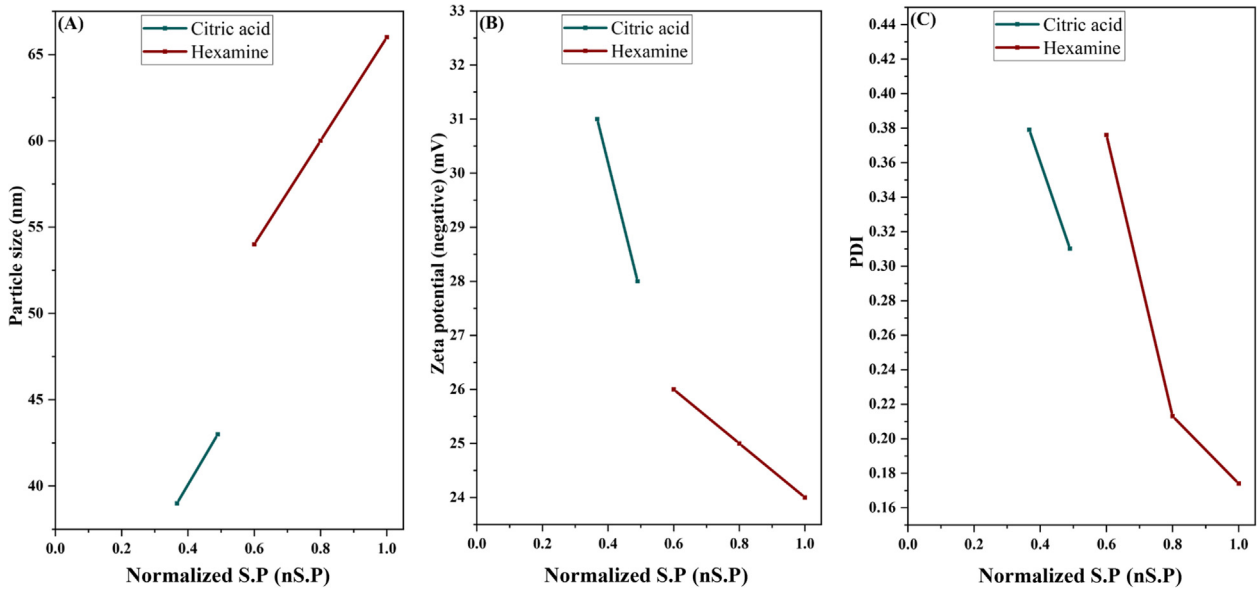

Fig. 6. The correlation between the results of particle size (A), zeta potential (R_t) (B), and poly dispersity index (PDI) (C) with the special point (S.P).

Table 6
The results of particle size, zeta potential, and PDI of the dispersed ZnO particles in the alcohol $^{*}p < 0.05$, $^{**}p < 0.01$, $^{***}p < 0.001$, and $^{****}p < 0.0001$). (The data of the amorphous samples (>70%) or the samples with impurities were not presented).

Fuel	F/O	Particle size nm	Zeta mV	PDI
Citric acid	0.75	39 ± 10	−31 ± 3	0.3790 ± 0.011
	1	43 ± 6 **	−28 ± 4 *	0.3101 ± 0.013 *
	1.25	–	–	–
Hexamine	0.75	54 ± 10 ***	−26 ± 2 **	0.3760 ± 0.011 ***
	1	60 ± 6	−25 ± 4	0.2130 ± 0.015
	1.25	66 ± 12 *	−24 ± 2 ***	0.1740 ± 0.001 ****
Hydrazine	0.75	45 ± 9 *	−28 ± 4 ***	0.3490 ± 0.019 ****
	1	53 ± 7	−22 ± 1	0.3550 ± 0.008
	1.25	76 ± 13 *****	−20 ± 2 **	0.2713 ± 0.013 ***
Urea	0.75	64 ± 4 *	−19 ± 4	0.2600 ± 0.013 *
	1	55 ± 9	−21 ± 5	0.2710 ± 0.023
	1.25	–	–	–

higher reaction rate, had smaller particle sizes than samples with higher S.P. As reported in the previous studies, the small particle size could change the surface charge and PDI of particles [39]. Besides, the increasing concentration of oxygen vacancies, which is commonly related to the outer surface of particles, could alter the surface charge of defective particles [39]. The results of zeta potential and PDI of the particle are presented in Table 6. Besides, the relation of zeta and PDI with S.P is shown in Fig. 6B and Fig. 6C, respectively. According to the data, the highest zeta potential (−31 mV) and the highest PDI values (0.3790) belong to the sample with the smallest particle size, i.e., the synthesized sample using citric acid at F/O = 0.75, which had the lowest S.P.

Optical properties

UV–visible spectra

UV–visible absorption spectroscopy is one of the most valuable techniques to determine the optical characteristics of semiconductor materials [4]. As reported in the previous studies, the synthesized ZnO particles with the SCS method with different fuels and F/O ratios have a wide range of band-gap (E_g) values from 3.06 to 3.47 [8]. As literature shows, the synthesis method, particle size, and structural defect concentrations could affect the band-gap values [40–42]. The estimated values of E_g of the synthesized samples using citric acid, hexamine, hydrazine, and urea are presented in Table 7. According to the data, in all samples, increasing the F/O ratio decreased the E_g values. In good agreement with Anitha et al. study [43], the E_g increased when the particle size increased (Table 6). The highest obtained E_g value was about 3.47 eV for the synthesized sample in the presence of hexamine at F/O = 1.25. Whereas the lowest E_g is about 3.06 eV for the synthesized sample using citric acid at F/O = 0.75. Besides, the difference between the band-gap values for synthesized ZnO powders in the presence of different fuels could be related to the remained fuels and partially doping of the structural groups of the fuels to ZnO structure, as reported in [4].

The relation between S.P and the E_g data in Fig. 7A, along with its relation with particle size in Fig. 6A, confirmed that in each group, the sample with the smallest particle size, which had the lowest nS.P, had the lowest value of E_g, as well. Another critical reason which reduced the E_g in samples with the low nS.P was the high concentration of oxygen vacancy defects in these samples. This subject is investigated in section 3.5.2.

Table 7
The results of estimated band-gap energy and magnetization saturation values of ZnO particles.

Fuel	F/O	E_g	M_s
Citric acid	0.75	3.06	0.01
	1	3.32	0.01
	1.25	–	–
Hexamine	0.75	3.11	0.05
	1	3.34	0.08
	1.25	3.47	0.20
Hydrazine	0.75	3.13	0.01
	1	3.15	0.11
	1.25	3.28	0.11
Urea	0.75	3.04	0.01
	1	3.08	0.08
	1.25	–	–

The correlation between E_g, the concentration of oxygen vacancy

The structural defects, especially the oxygen vacancies, could change the optical properties of the semiconductors [44–46]. The correlation between the optical band-gap and the concentration of the oxygen vacancies was predicted using the DFT method (Fig. 7B). According to the results, E_g values steadily decreased when the concentration of oxygen vacancies increased. The obtained data from the Kermani model (Table 4) and the E_g data demonstrated the same results; the synthesized samples with a high concentration of oxygen vacancies (low S.P) had low band-gap values. This relation could also be explained by considering the possibility of creating a new trap band in ZnO particles containing oxygen vacancies (Fig. 7C).

Magnetic measurements

The M_s values of synthesized ZnO powders are shown in Table 7. According to Table 7, it can be said that the synthesized ZnO particles had a weak magnetic property. The results indicated that increasing the F/O ratios in all systems improved the M_s values. The M_s value of combusted samples was in the range of 0.01–0.2 emu/g. The highest M_s (0.2 emu/g) belongs to the synthesized sample in the presence of hexamine at F/O = 1.25 (see Fig. 8A).

The obtained M_s values in this study are interestingly higher than the previously reported results. Ma et al. investigated the effect of oxygen-deficient ZnO on the magnetic properties, which were synthesized via the sol–gel route. Different annealing processes for adsorption and desorption of oxygen have been done to synthesis an oxygen-deficient ZnO structure. The maximum reported M_s value was about 0.001 emu/g at room temperature [47]. Such enhancement in the M_s values could be explained by the results of Sections 3.1–3.3, along with the results of previous studies [9]. It is documented that oxygen vacancies, as well as the other defects, are the crucial factors that affect the M_s values [5]. Referring to the thermodynamic aspects (see Section 3.1) and the results of the concentration of oxygen vacancy evaluation, it can be inferred that the intense combustion process accompanied by a rapid cooling process results in the enhancement of M_s value to 0.2 emu/g. Different values of M_s for the synthesized samples in the presence of various fuels could be related to partially doping of structural groups of fuels to ZnO structure (e.g., N-doping ZnO, Fig. S2) that could be changed the magnetic moments. Besides, the atomic Zn might be partially doped to ZnO structure and/or substituted with O atom ($Zn_{1+x}O_{1-x}$), resulting in the magnetization of ZnO due to Bohr magneton of metallic Zn^{2+} atom(s).

According to the direct relation of S.P and M_s values (Fig. 8B), and comparing the results with Section 3.1–3.3, it can be said that when the concentration of interfered O_2 decreased, the M_s values increased.

Emission color

The previous studies indicated that the formation of structural defects could change the color of synthesized oxide particles in a wide range, i.e., from white to black [11]. The colorimetry test was performed using Commission International del' Eclairage 1931 (CIE 1931) functions. The CIE 1931 graphs of the synthesized ZnO particles are shown in Fig. 9A and B. Table 8 also shown the corresponding CIE coordinates and correlated color temperature. All sample coordination's are almost match with the expected white light-emitting region. It is noted that the area with coordination of x = 0.28–0.35 and y = 0.30–0.37 is related to the region with balanced white light [4]. According to the presented data in Fig. 9, the color hue was changed from white to pink and yellow–red via increasing the F/O vales in all samples. Considering Fig. 9 and S.P data in Table 4, it can be said that for each fuel, the samples, which were synthesized at lower nS.P, had a darker color than the sam-

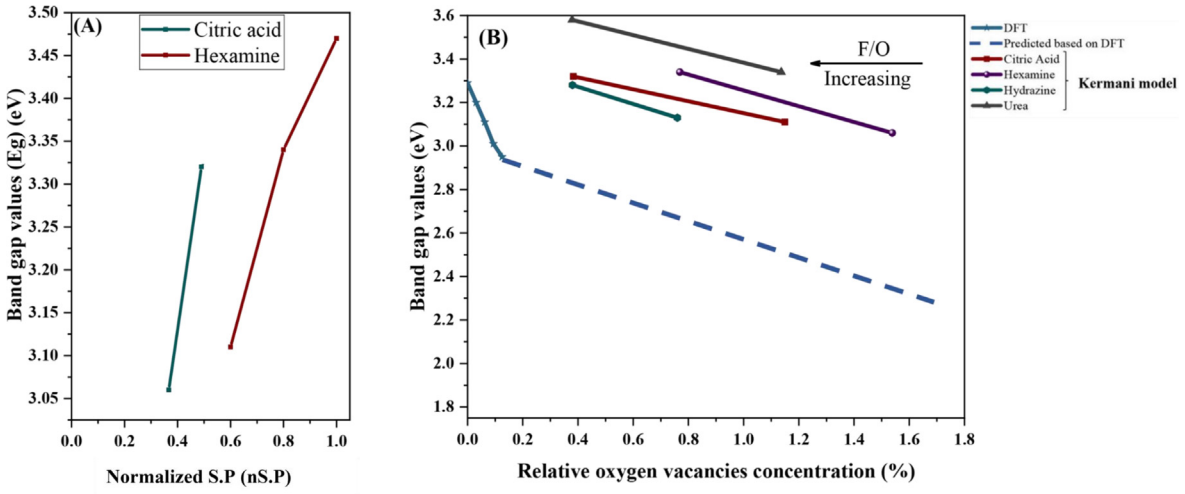

Fig. 7A. The correlation between the band gap (E_g) values and the special point (S.P) (A). The correlation between the density functional theory (DFT), E_g data of the synthesized ZnO, and the calculated concentration of oxygen vacancy defects with the Kermani model [10] (B).

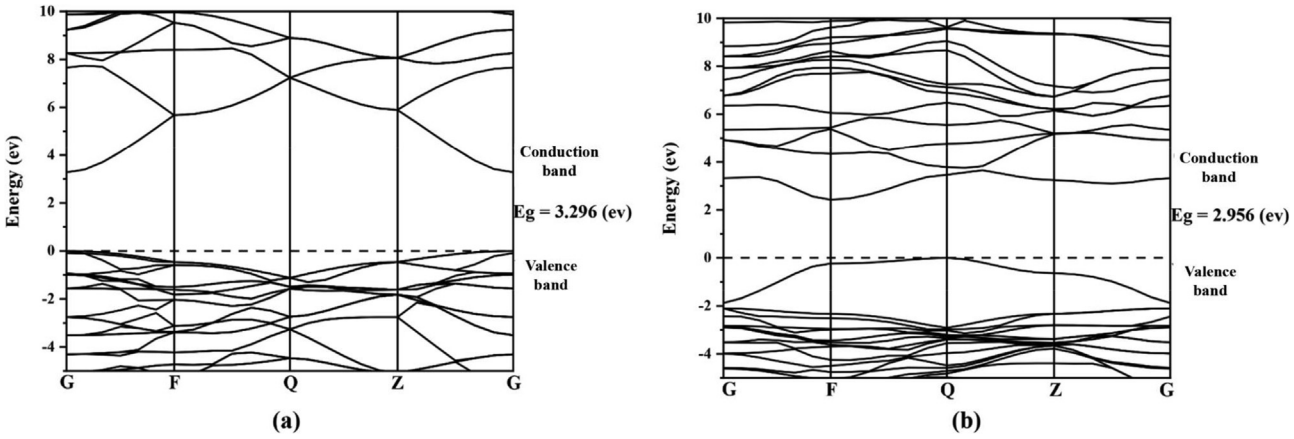

Fig. 7C. The different conduction band energy levels of ZnO particles with different concentrations of oxygen vacancy defects, which was calculated using density functional theory (DFT).

ples synthesized at higher nS.P. The observed color difference could be due to the different concentrations of structural defects in different samples. The synthesized samples at lower S.P contained a higher concentration of oxygen vacancies than the samples synthesized at higher S.P values, as shown in Section 3.1.2.

The morphology of synthesized samples

Particles that are produced by the SCS method commonly have porous structures with non-uniform shapes [48]. The morphology of ZnO powders, synthesized at F/O = 1 with citric acid, hexamine, hydrazine, and urea, are shown in Fig. 10A–D, respectively. Agglomerated ZnO particles with flower-like morphology were seen in Fig. 10 in all synthesized ZnO powders. As the literature showed, ZnO with a nano flower structure is suggested as a promising candidate as an antibacterial agent [49–51].

Antibacterial activity evaluations

ZnO is considered a non-toxic and biocompatible antibacterial agent according to the previous *in vitro* and *in vivo* results [52,53]. The antibacterial activity of the SCS synthesized ZnO particles might be altered regarding different morphology, particle

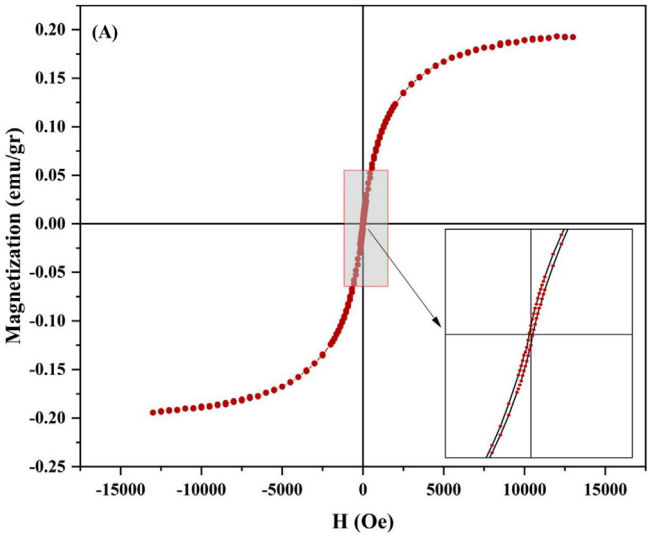

Fig. 8A. Vibrating-sample magnetometer results of the synthesized ZnO particles in the presence of hexamine at F/O = 1.25.

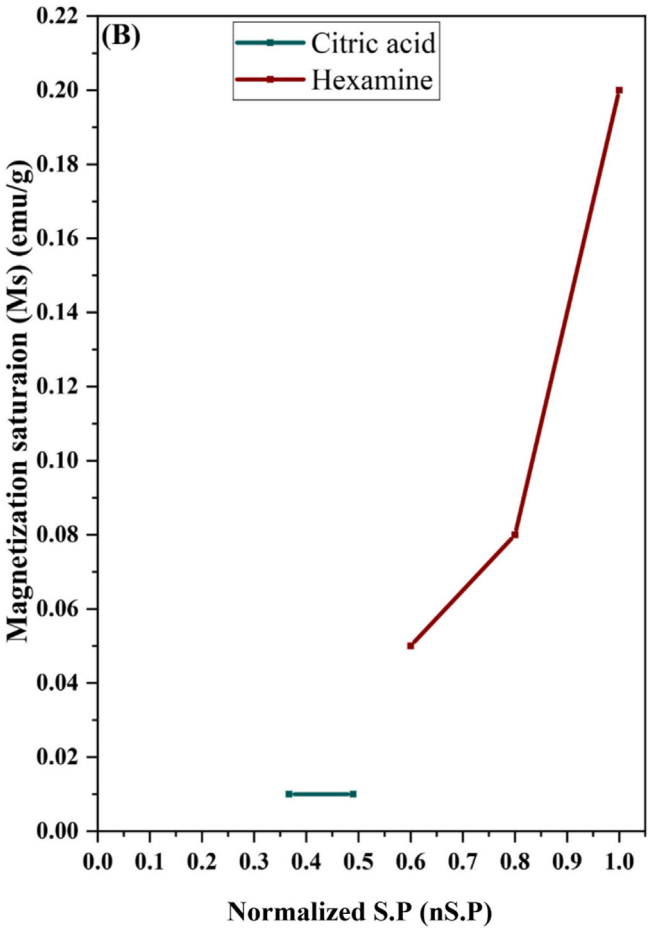

Fig. 8B. The correlation between the magnetization saturation (M_s) values and special point (S.P) of the synthesized ZnO particles.

size, crystallinity, and concentration of defects of the SCS products. Consequently, the antibacterial activity of the samples should be clarified. Accordingly, the inhibitory effects of synthesized ZnO particles against Gram-negative bacteria (E. coli) and Gram-positive bacteria (S. aureus) were studied using the MIC method, and the results are presented in Fig. 11A-–F–. According to Fig. 11A, the highest E. coli death is related to the treated bacteria with the synthesized samples at F/O = 0.75. The E. coli growth-

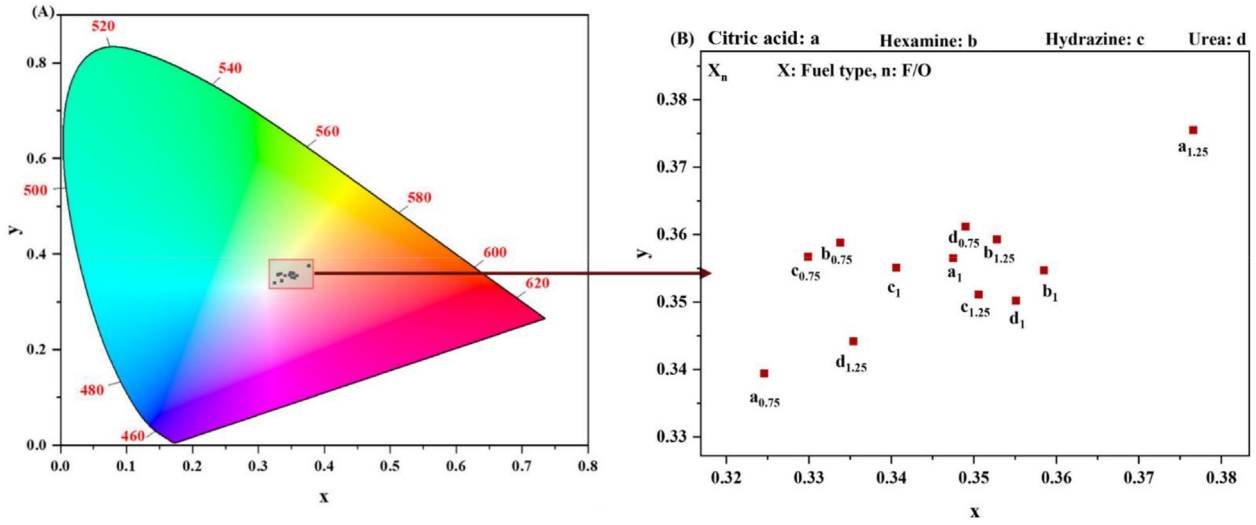

Fig. 9. A and B: Commission International del' Eclairage 1931color matching functions of the synthesized ZnO particles.

Table 8
The results of CIE coordinates and correlated color temperature of the ZnO particles.

Fuel	F/O	CIE coordinates	
		x	*y*
Citric acid	0.75	0.3246	0.3394
	1	0.3475	0.3565
	1.25	–	–
Hexamine	0.75	0.3338	0.3338
	1	0.3528	0.3593
	1.25	0.3406	0.3551
Hydrazine	0.75	0.3299	0.3567
	1	0.3506	0.3511
	1.25	0.3585	0.3547
Urea	0.75	0.3490	0.3612
	1	0.3551	0.3502
	1.25	–	–

inhibitory of the synthesized samples with citric acid and hexamine is about 88 and 80%, respectively, in the concentration of 15.625 μg/ml. According to Fig. 11B and C, the *E. coli* growth-inhibitory of the synthesized sample at F/O = 1 and F/O = 1.25 is significantly reduced. The highest antibacterial activity against *E. coli* in the synthesized sample at F/O = 1 and F/O = 1.25 is related to citric acid, which was equal to 49 and 37%, respectively. Besides, the highest growth inhibitory against *S. aureus* at F/O = 0.75, 1, and 1.25 was equal to 100, 84, and 74%, respectively, in the synthesized sample in the presence of citric acid. The most important mechanism of antibacterial activity of ZnO powder is the generation of reactive oxygen species (ROS) (e.g., O_2^*, OH^*, and H_2O_2) on the surface. In this mechanism, produced ROS is penetrated to bacteria's cell wall, resulting in the bacteria cell devastation [45,54]. Besides, the release of Zn^{2+} in the biological environment and direct contact of ZnO with the cell membrane of bacteria could reduce the surface tension of bacterium plasma and destroyed the bacteria cell wall [54].

The comparison of the presented antibacterial data in Fig. 11 and the S.P data (Table 3) demonstrates a remarkable result as follows:

Synthesized samples in the lower nS.P in each group have more potential for antibacterial activity against Gram-negative and Gram-positive bacteria. According to the data, the synthesized samples with the lower nS.P have a higher concentration of oxygen vacancy defects (see Section 3.1.3), smaller particle size, higher surface charge (see Section 3.4), and lower band-gap values (see Section 3.5) in comparison to the synthesized samples with the lower nS.P. Accordingly, these samples (synthesized sample at the lower S.P) could possess' higher antibacterial activity. The lower antibacterial inhibitory in the presence of hydrazine and urea might be related to the residual fuels in these systems with negative values of S.P in comparison to other samples.

It's noted that the Gram-negative bacteria have more resistance than the Gram-positive bacteria against the synthesized ZnO powders. Many previous studies also indicated the better influence of ZnO against Gram-positive bacteria [54]. This subject stems from the different cell wall structures, cell physiology, and metabolism death of Gram-positive and Gram-negative bacteria [54].

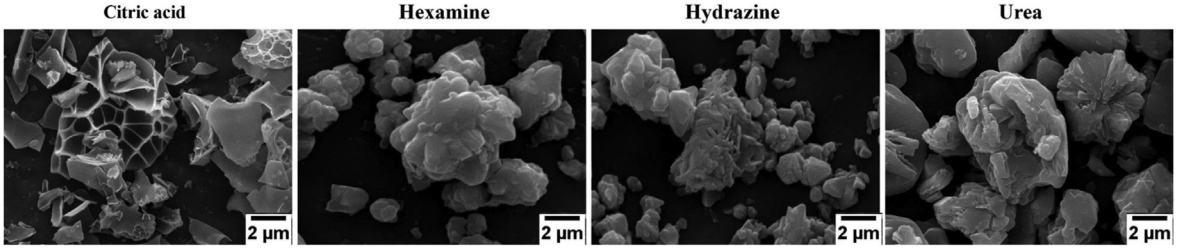

Fig. 10. Scanning electron microscopy (SEM) images of the synthesized ZnO particles in F/O = 1.

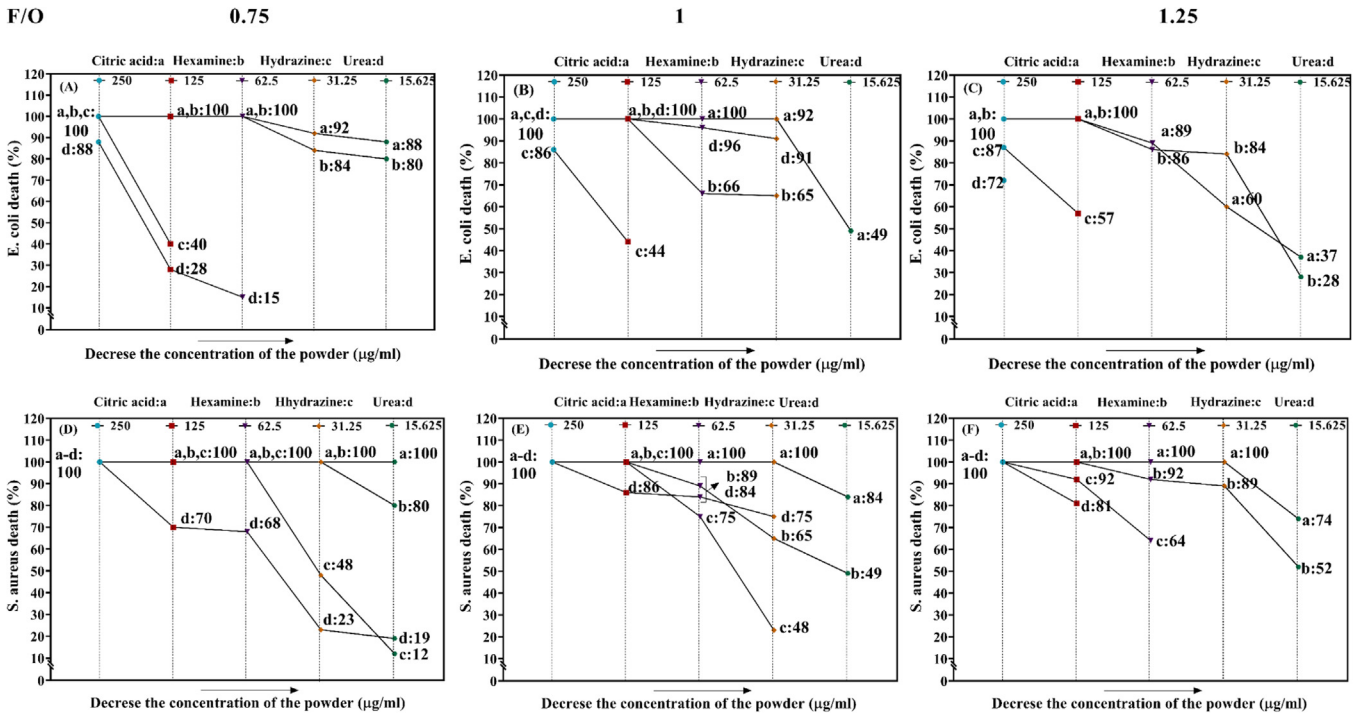

Fig. 11. The results of minimum inhibitory concentration (MIC) of the synthesized ZnO particles.

Conclusion

In this study, some theoretical calculations were used to determine the special ratio of reducing to oxidizing elements (S.P), which led to the maximum interference of O_2 during combustion reaction. The relation between S.P and the properties of different SCS synthesized ZnO powder was explored. The correlation of S.P and the concentration of oxygen vacancy defects, which are commonly available in the SCS products, was surveyed via the DFT method. The most desirable properties of the synthesized sample belonged to the ZnO powders, which were synthesized in the presence of citric acid with an S.P of 0.355. The mentioned sample had promising crystallite size (48 nm), particle size (39 nm), zeta (−31 mV), PDI (0.3760), band-gap (3.06 eV), and MIC against E. coli and S. aureus (15.625 μg/mL) values. The calculation of S.P before the synthesis process could provide a general overview of the SCS products' properties.

Author Contributions

Conceptualization and Resource: S. Mollazadeh; Experimental investigation: E. Garmroudi; Writing Original Draft Preparation, Editing the data, Software and theoretical investigation: F. Kermani; Density functional theory (DFT) calculation: Z. Mollaei; Review & Editing: S. Mollazadeh., M. Mashreghi, and J. Vahdati Khakhi. All authors have read and agreed to the published version of the manuscript.

Funding

This research was supported by a financial grant from the Ferdowsi University of Mashhad (No. 2/49558).

Declaration of Competing Interest

The authors declare that they have no known competing financial interests or personal relationships that could have appeared to influence the work reported in this paper.

Acknowledgment

The authors would like to acknowledge the assistance and support of the Outotec team (Espoo, Finland) in providing the HSC chemistry software, Cambridge Enterprise Limited in providing CASTEP software, and Cambridge Crystallographic Data Centre (CCDC)) in providing Mercury software.

Appendix A. Supplementary data

Supplementary data to this article can be found online at https://doi.org/10.1016/j.jiec.2021.11.047.

References

[1] F. Kermani, S. Mollazadeh, S. Kargozar, J. Vahdati Khakhi, Mater. Sci. Eng. C 118 (2021) 1–28, https://doi.org/10.1016/j.msec.2020.111533.
[2] F. Kermani, A. Gharavian, S. Mollazadeh, S. Kargozar, A. Youssefi, J. Vahdati Khaki, Mater. Sci. Eng. C 111(2019) (2020) 110828. 10.1016/j.msec.2020.110828.
[3] S. Mandizadeh, F. Soofivand, M. Salavati-Niasari, S. Bagheri, J. Ind. Eng. Chem. 26 (2015) 167–172, https://doi.org/10.1016/j.jiec.2014.10.044.
[4] H. Kazemi, F. Kermani, S. Mollazadeh, J. Vahdati Khakhi, Int. J. Appl. Ceram. Technol. 17(4) (2020) 1852–68. 10.1111/ijac.13515.
[5] H. Aali, S. Mollazadeh, J.V. Khaki, Ceram. Int. 44 (16) (2018) 20267–20274, https://doi.org/10.1016/j.ceramint.2018.08.012.
[6] A.V. Saghir, S.M. Beidokhti, J.V. Khaki, A. Salimi, J. Eur. Ceram. Soc. 41 (1) (2021) 563–579, https://doi.org/10.1016/j.jeurceramsoc.2020.08.044.
[7] H. Aali, N. Azizi, N.J. Baygi, F. Kermani, M. Mashreghi, A. Youssefi, et al., Ceram. Int. 45 (15) (2019) 19127–19140, https://doi.org/10.1016/j.ceramint.2019.06.159.
[8] A. Varma, A.S. Mukasyan, A.S. Rogachev, K.V. Manukyan, Chem. Rev. 116 (23) (2016) 14493–14586, https://doi.org/10.1021/acs.chemrev.6b00279.

[9] F. Kermani, S. Mollazadeh, J. Vahdati Khaki, Ceram. Int. 45(10) (2019) 13496–501. 10.1016/j.ceramint.2019.04.053.
[10] H. Aali, S. Mollazadeh, J.V. Khaki, Ceram. Int. 45 (14) (2019) 17775–17783, https://doi.org/10.1016/j.ceramint.2019.05.348.
[11] F. Kermani, S. Mollazadeh, S. Kargozar, J.V. Khakhi, Mater. Sci. Eng. C 124 (2021), https://doi.org/10.1016/j.msec.2021.112082 112082.
[12] H. Aali, N.J. Baygi, S. Mollazadeh, J.V. Khaki, Ceram. Int. (2021), https://doi.org/10.1016/j.ceramint.2021.03.233.
[13] A.S. Ansari, J.W. Han, B. Shong, J. Ind. Eng. Chem. 96 (2021) 236–242, https://doi.org/10.1016/j.jiec.2021.01.016.
[14] Z.K. Ghouri, A. Badreldin, K. Elsaid, D. Kumar, K. Youssef, A. Abdel-Wahab, J. Ind. Eng. Chem. 96 (2021) 243–253, https://doi.org/10.1016/j.jiec.2021.01.027.
[15] R. Aslam, M. Mobin, Huda, M. Shoeb, M. Murmu, P. Banerjee, J. Ind. Eng. Chem. 100 (2021) 333–350, https://doi.org/10.1016/j.jiec.2021.05.005.
[16] M. Hao, M. Qiu, H. Yang, B. Hu, X. Wang, Sci. Total Environ. 760 (2021), https://doi.org/10.1016/j.scitotenv.2020.143333 143333.
[17] L. Yao, H. Yang, Z. Chen, M. Qiu, B. Hu, X. Wang, Chemosphere 273 (2021), https://doi.org/10.1016/j.chemosphere.2020.128576 128576.
[18] M. Qiu, B. Hu, Z. Chen, H. Yang, L. Zhuang, X. Wang, Biochar 3 (2) (2021) 117–123, https://doi.org/10.1007/s42773-021-00098-y.
[19] M. Alavi, N. Karimi, I. Salimikia, J. Ind. Eng. Chem. 72 (2019) 457–473, https://doi.org/10.1016/j.jiec.2019.01.002.
[20] A. Das, N. S.K., R.G. Nair, Nano-struct. Nano-objects 19 (2019) 100353. 10.1016/j.nanoso.2019.100353.
[21] T.C. Bharat, Shubham, S. Mondal, H.S. Gupta, P.K. Das, A.K. Singh, Mater. Today Proc. 11 (2019) 767–775, https://doi.org/10.1016/j.matpr.2019.03.041.
[22] L. Huang, Y. Hao, M. Hu, Mater. Sci. Semicond. Process. 74(June 2017) (2018) 303–8. 10.1016/j.mssp.2017.08.032.
[23] T.K. Pathak, A. Kumar, C.W. Swart, H.C. Swart, R.E. Kroon, RSC Adv. 6 (100) (2016) 97770–97782, https://doi.org/10.1039/c6ra22341a.
[24] A. Roine, (2019).
[25] A. Fathi, F. Kermani, A. Behnamghader, S. Banijamali, M. Mozafari, F. Baino, et al., Biomed. Glas. 6 (1) (2021) 57–69, https://doi.org/10.1515/bglass-2020-0006.
[26] Y. Wang, D. Puggioni, J.M. Rondinelli, 115149 (2019) 1–15. 10.1103/PhysRevB.100.115149.
[27] K. Choudhary, F. Tavazza, Comput. Mater. Sci. 161 (2019) 300–308, https://doi.org/10.1016/j.commatsci.2019.02.006.
[28] P. Wisesa, K.A. Mcgill, T. Mueller, 155109(April) (2016) 1–10. 10.1103/PhysRevB.93.155109.
[29] S.S.R.K.C. Yamijala, Z.A. Ali, B.M. Wong, J. Phys. Chem. C 123(41) (2019) 25113–20. 10.1021/acs.jpcc.9b03554.
[30] B. Meyer, D. Marx, J. Phys. Condens. Matter 15 (2) (2003) 89–94, https://doi.org/10.1088/0953-8984/15/2/112.
[31] S.H. Jin, Y. Yoon, Y. Jo, S.Y. Lee, H.S. Moon, S. Seok, et al., J. Ind. Eng. Chem. 96 (2021) 376–381, https://doi.org/10.1016/j.jiec.2021.01.046.
[32] X. Zhang, Y. Han, W. Liu, N. Pan, D. Li, J. Chai, J. Ind. Eng. Chem. 97 (2021) 326–336, https://doi.org/10.1016/j.jiec.2021.02.019.
[33] S. Kunj, J. Ind. Eng. Chem. 92 (2019) (2020) 145–157, https://doi.org/10.1016/j.jiec.2020.08.033.
[34] S. Kunj, K. Sreenivas, J. Ind. Eng. Chem. 60 (2018) 151–159, https://doi.org/10.1016/j.jiec.2017.10.051.
[35] Z. Mollaei, F. Kermani, F. Moosavi, S. Kargozar, J.V. Khakhi, S. Mollazadeh, Ceram. Int. (2021), https://doi.org/10.1016/j.ceramint.2021.09.245.
[36] T.K. Pathak, H.C. Swart, R.E. Kroon, Spectrochim. Acta - Part A Mol. Biomol. Spectrosc. 190 (2018) 164–71. 10.1016/j.saa.2017.09.026.
[37] R. Ianoș, R. Lazău, R.C. Boruntea, Ceram. Int. 41 (2) (2015) 3186–3190, https://doi.org/10.1016/j.ceramint.2014.10.171.
[38] R. Ianoș, M. Bosca, R. Lazău, Ceram. Int. 40 (Part B) (2014) 10223–10229, https://doi.org/10.1016/j.ceramint.2014.02.110.
[39] F. Kermani, S.M. Beidokhti, F. Baino, Z. Gholamzadeh-Virany, M. Mozafari, S. Kargozar, Materials (Basel) 13 (6) (2020) 1348, https://doi.org/10.3390/ma13061348.
[40] S. Kumar Ray, J. Hur, J. Ind. Eng. Chem. 101 (2021) 28–50, https://doi.org/10.1016/j.jiec.2021.06.027.
[41] D. Hun Kim, S. Jae Jeon, Y. Woon Han, Y. Hoon Kim, N. Gyu Yang, H. Seok Lee, et al., J. Ind. Eng. Chem. 101 (2021) 135–143, https://doi.org/10.1016/j.jiec.2021.06.020.
[42] M.A. Hossain, S. Jeon, J. Ahn, H. Joh, J. Bang, S.J. Oh, J. Ind. Eng. Chem. 73 (2019) 214–220, https://doi.org/10.1016/j.jiec.2019.01.027.
[43] S. Anitha, S. Muthukumaran, Mater. Sci. Eng. C 108 (2020), https://doi.org/10.1016/j.msec.2019.110387 110387.
[44] S. Chen, Y. Xiao, Y. Wang, Z. Hu, H. Zhao, W. Xie, Nanomaterials 8 (4) (2018) 1–16, https://doi.org/10.3390/nano8040245.
[45] Y. Nosaka, A.Y. Nosaka, Chem. Rev. 117 (17) (2017) 11302–11336, https://doi.org/10.1021/acs.chemrev.7b00161.
[46] H.S. Sindhu, B.V. Rajendra, N.D. Hebbar, S.D. Kulkarni, P.D. Babu, J. Lumin. 199 (2018) 423–432, https://doi.org/10.1016/j.jlumin.2018.03.054.
[47] N. Ma, Y. Zhang, E. Cao, L. Sun, W. Hao, Z. Yang, 727(January) (2019) 6–10. 10.1016/j.cplett.2019.04.049.
[48] N.J. Baygi, A.V. Saghir, S.M. Beidokhti, J.V. Khaki, Ceram. Int. 46 (10) (2020) 15417–15437, https://doi.org/10.1016/j.ceramint.2020.03.087.
[49] J. Kim, Y. Im, K.S. Park, T.W. Cho, J. Jeon, K. il Chung, M. Kang, J. Ind. Eng. Chem. 56 (2017) 463–471, https://doi.org/10.1016/j.jiec.2017.07.044.
[50] Y. Bao, L. Gao, C. Feng, J. Ma, W. Zhang, C. Liu, et al., J. Ind. Eng. Chem. 82 (2020) 180–189, https://doi.org/10.1016/j.jiec.2019.10.011.
[51] J. Yoon, S.G. Oh, J. Ind. Eng. Chem. 96 (2021) 390–396, https://doi.org/10.1016/j.jiec.2021.01.043.
[52] A. Kolodziejczak-Radzimska, T. Jesionowski, Materials (Basel). 7 (4) (2014) 2833–2881, https://doi.org/10.3390/ma7042833.
[53] D.N. Phan, R.A. Rebia, Y. Saito, D. Kharaghani, M. Khatri, T. Tanaka, et al., J. Ind. Eng. Chem. 85 (2020) 258–268, https://doi.org/10.1016/j.jiec.2020.02.008.
[54] A. Sirelkhatim, S. Mahmud, A. Seeni, Nano-Micro Lett. 7 (2015) 219–242, https://doi.org/10.1007/s40820-015-0040-x.